Field-induced orbital patterns in ferromagnetic layered ruthenates

Filomena Forte, Mario Cuoco, and Canio Noce
CNR-SPIN, Fisciano, I-84084 Salerno, Italy
and Dipartimento di Fisica "E. R. Caianiello" Università di Salerno, Fisciano, I-84084 Salerno, Italy
(Received 18 June 2008; revised manuscript received 14 September 2010; published 5 October 2010)

We study the evolution of orbital patterns in ferromagnetic layered ruthenates due to the competition of Coulomb interactions, compressive c axis and orthorhombic distortions in the presence of a polarizing orbital field coupled to the angular momentum. By means of the exact diagonalization on a 2×2 cluster and a cluster embedded analysis where interplaquette interaction is treated on mean-field level, we determine the ground-state phase diagram. Specifically, we demonstrate that, via the activation of two or three of t_{2g} local orbital configurations, an external field applied along different symmetry directions can lead to inequivalent orbital correlated states. Starting from an antiferro-orbital pattern, for the easy axis case an orbital ordered phase is induced, having strong next-nearest-neighbors ferro-orbital correlations. Otherwise, a field applied along the hard axis leads a reduction in local orbital moment in a way to suppress the orbital order.

DOI: 10.1103/PhysRevB.82.155104 PACS number(s): 74.70.Pq, 71.10.−w, 75.10.−b, 75.50.Ee

I. INTRODUCTION

Large Coulomb repulsion, orbital degeneracy and lattice distortions are widely accepted to be key parameters in determining the intriguing and fascinating phenomena of transition metal oxide materials.[1–3] Colossal magnetoresistance (CMR) in perovskitic manganites is one of the most significant examples of the subtle competition between spin-orbital-charge degrees of freedom at the borderline between different types of ordered states.[4,5]

Moreover, when electrons in degenerate d shells localize in Mott-Hubbard or charge transfer insulators, unusual collective behaviors may emerge as a consequence of the orbital frustration on the spin degree of freedom. In this context, quantum effects associated with the orbital degree of freedom are expected to be of great relevance both for e_g (Refs. 6 and 7) and t_{2g} systems.[8,9]

Recently, the physics of $Ca_3Ru_2O_7$ compound has attracted a lot of interest due to a novel type of observed CMR (Refs. 10–15) that is likely to be driven by orbital rather than quantum spin effects. This compound belongs to the Ruddlesden-Popper series $Ca_{n+1}Ru_nO_{3n+1}$, n being the number of Ru-O layers per unit cell and thus exhibits a bilayered structure. The crystal structure is orthorhombic with significant distortions in the ac plane due to the tilting of RuO_6 octahedra around the b axis.[16] In zero field, $Ca_3Ru_2O_7$ undergoes an antiferromagnetic (AFM) transition at $T_N=56$ K while remaining metallic and then a Mott-type transition at $T_{MI}=48$ K with a dramatic reduction (up to a factor of 20) in the conductivity for $T<T_{MI}$.[10,11,13,14,17] This transition is accompanied by an abrupt shortening of the c axis lattice parameter below T_{MI}.[10,18] We notice that in the AFM state, neutron-scattering measurements indicate that the magnetic moments align ferromagnetically within the double layer, and antiferromagnetically between the double layers (A-type AFM structure) along the c axis.[19,20]

Concerning the mechanism behind the CMR in $Ca_3Ru_2O_7$, the physics involved is likely to be fundamentally different from that governing all other magnetoresistive materials. Experiments reveal that the electronic transport is so deeply interrelated to the spin-orbital correlations that, if one applies a magnetic field along the magnetization easy-axis a,[21] there occurs a first-order metamagnetic transition to a spin-polarized state, without leading to a full suppression of the insulating state. Otherwise, the most favorable magneto-conducting state is driven by the field directed along the hard-axis b, where most likely an orbital disordered phase regime is obtained, without considerably affecting the magnetic structure. Indeed, in this regime the magnetization does not change significantly, thus suggesting that magnetic scattering is not the primary mechanism responsible for CMR.[11,13,19,22] These transitions are also accompanied by anisotropic structural changes and modifications of the coupling between the electrons and the lattice.[13–15,18] Notably, when the field is applied along the low temperature hard axis, there occurs a sharp structural change that ties the CMR to an increase in the c-axis lattice parameter.[18] The joining together of CMR, structural changes and metal-insulator transition is a clear indication of the interplay between spin, charge and lattice degrees of freedom.[23]

Earlier theoretical studies on the phenomenology occurring in $Ca_3Ru_2O_7$ have been devoted to understand the nature of the antiferromagnetic metallic state[24,25] and the character of the metal-insulator transition.[26] The crucial role of orbital degrees of freedom and structural distortions has been recently recognized in the conducting behavior of $Ca_3Ru_2O_7$ (Ref. 27) while it has been extensively analyzed in the single layered compound Ca_2RuO_4, where it has gained a lot of extra interest in the context of orbital-selective Mott transitions.[28–31]

Having in mind the experimental scenario above mentioned for $Ca_3Ru_2O_7$, the nature of the ground state within the layered ferromagnetic insulating state turns out to be a relevant issue to be addressed. In this case since the spin and charge degrees of freedom can be projected out, a suitable microscopic description has to explicitly include the degeneracy of t_{2g} orbital sector, the compressive c axis and the orthorhombic distortions of RuO_6 octahedra. Then, as for other correlated insulating states, we base the low-energy description on an effective orbital only model in the regime of strong on site Coulomb repulsion. Due to the many com-

peting couplings involved in the problem, the analysis of the orbital correlations within the different ground states is performed via a systematic approach. First, the given model Hamiltonian is solved by means of exact diagonalization (ED) technique on a 2×2 plaquette. This analysis provides an unbiased insight on the character of the ground-state (GS) configurations as the microscopic interactions are treated without any approximation and on equal footing. Then, considering an embedded cluster approach where the intraplaquette Hamiltonian is solved via ED while the interplaquettes interaction is treated within a self-consistent mean-field (MF) approximation, we extract the phase diagram for the allowed broken symmetry configurations.

There are two main aspects behind the general complexity of the problem we faced; (i) the Heisenberg-type Hamiltonian for pseudospin-1 that we considered is marked by directional exchanges that in two dimensions, due to the peculiar connectivity via the oxygen ligands of the t_{2g} centers, lead to antiferromagnetic correlations that are highly frustrated; (ii) the tetragonal and the orthorhombic crystal field terms act like effective orbital fields that do not commute between each other. In this respect, even considering the case of a $S=1/2$ antiferromagnetic Heisenberg Hamiltonian, one can notice that the application of two noncommuting fields would produce a problem that cannot be solved exactly even in one dimension.[32–34] We underline that our orbital case refers to a spin-1 like system thus it intrinsically contains extra degrees of freedom whose interplay with the presence of two-noncommuting fields adds extra difficulties and different scenarios as compared to the spin-1/2 situation.

In particular, the octahedral distortions lift the pristine orbital degeneracy and set orbital patterns that privilege exchange along the easy axis a. This corresponds to lowering the local number of active degrees of freedom, that is reduced to the only two orbital configurations that can be effectively connected along the selected direction. Given this scenario, we show that the application of the field along the hard axis restores the local orbital fluctuations among the whole t_{2g} subspace, by reintroducing the extra configuration that was quenched by the balance between orbital exchange and crystal-field amplitudes.

Special attention is devoted to analyzing the consequences of activating two or three of the t_{2g} local-orbital configurations on the evolution of orbital order. One of the main findings is that a polarizing orbital field destabilizes antiferro-orbital ordered (OO) phases, both when applying the field along the easy or the hard axis. However, we show that depending on the axial direction, we get two fundamentally different mechanisms: for a field applied along the easy axis a, the effect of the field is mainly to reorient the orbital moments inducing ferro-orbital correlations in the direction of the transverse applied field. Due to the orbital configurations involved, this situation still has the features of an orbitally ordered state, where nearest-neighbor antiferro-orbital correlations are strongly suppressed. On the contrary, in the hard axis b case, the activated configuration along b reduces the amplitude of the ordering orbital moments in zero field up to reach an orbital disordered phase.

We finally consider possible connections between the symmetry breaking associated with the orbital ordered state and the peculiar magnetoconducting behavior of layered ruthenates.

The paper is organized in the following way: in the next section we introduce and write down the microscopic model; in Sec. III we present, for a 2×2 plaquette, the numerical results obtained for the phase diagram as function of the microscopic parameters stressing the role played by the purely structural distortions and their interplay with external magnetic field while in Sec. IV we present embedded mean-field calculations based on exact diagonalization of 2×2 plaquette; the last section contains a discussion of the results presented and the conclusions.

II. EFFECTIVE ORBITAL MODEL

Based on the assumption that the planar spin configuration is not substantially modified by the applied field, we consider the coupling between the field and the local-orbital angular momentum contribution as the dominant one. In particular, starting from different OO ground states at zero field, we will study how these configurations are modified as a consequence of the induced orbital "flip" via the coupling between the applied field and the orbital angular momentum along different symmetry in-plane directions. Then, by means of these results, we will consider the evolution of the ground state under the external field, and in turn use such investigation to discuss the possible implications with respect to the anomalous CMR phenomenon observed in the $Ca_3Ru_2O_7$.

As mentioned in Sec. I, to investigate the correlations developing within the orbital sector, we start from a situation where the system is fully polarized and all the spins are aligned along a given crystallographic direction, in accordance to the observed A-type configuration. In this frame, the attention is focused on the orbital degree of freedom, out of the competition between the Coulomb repulsion (orbital exchange), octahedral distortions, and the effect of the orbital field. In particular, having in mind the Ca-based ruthenates, the case of flat octahedral configuration with orthorhombic distortions is considered. In such a scheme we can explore the interplay between orbital exchange and the quenching of orbital correlations provided by structural distortions. The specific model Hamiltonian we refer to is built up by the following contributions:

$$H = H_{exc} + H_{tet} + H_{ort} + H_{\alpha}, \tag{1}$$

where H_{exc} stands for the orbital exchange interaction, H_{tet} and H_{ort} are the crystalline fields terms, describing local c-axis tetragonal distortions and in-plane orthorhombic deformations, respectively, and H_{α} represents the coupling of the orbital angular momentum to the external field.

The first term in Eq. (1) is derived from the superexchange Hamiltonian for $S=1$ spins and it is able to describe, in the low-energy limit, the interaction arising from the virtual excitation between two neighboring sites. In a previous work,[35] we have proved that such a description, which has the same roots as the superexchange in a Mott insulator with nondegenerate orbitals,[7] can be applied to the case of ruthenates, being consistent with a significant value of an on-site intraorbital Coulomb interaction.

In ruthenates, the Hund's coupling is larger than the crystal field splitting of t_{2g} subspace and the Ru^{4+} ions are in triplet configuration. Dealing with an atomic t_{2g}^4 configuration, the superexchange interaction arises from virtual processes $\langle i,j\rangle$ of the type $d_i^4 d_j^4 \rightarrow d_i^5 d_j^3 \rightarrow d_i^4 d_j^4$. Each of the orbitals involved is orthogonal to one cubic axis; for instance, d_x is orthogonal to the x axis while d_y and d_z are orthogonal to y and z, respectively. Due to the connectivity via intermediate oxygen ligands, only two out of the three t_{2g} orbitals can be effectively connected for each axial direction.

The spin/orbital model for Ca-ruthenates can be directly derived from the one adopted for cubic vanadates,[8] by performing a particle-hole transformation within the t_{2g} sector, in a way to map the problem of four electrons to that of two holes and consequently the doublon states in "no hole" configurations. In this way, we reduce ourselves to consider virtual excitations of the kind $d_i^2 d_j^2 \rightarrow d_i^3 d_j^1 \rightarrow d_i^2 d_j^2$.

Here, we refer to a simplified version of the Hamiltonian in Ref. 35, obtained under the assumption $J_H/U \rightarrow 0$, J_H being the Hund's coupling and U the (large) Coulomb interaction. Moreover, in the present case, the spin degrees of freedom have been projected out, by assuming a fully polarized planar configuration, where $\langle S_i \cdot S_j \rangle = 1/4$. The orbital exchange Hamiltonian is then written as follows:

$$H_{exc} = \frac{1}{2} J \sum_{\gamma} \sum_{\langle ij \rangle \| \gamma} \left[\vec{\tau}_i \cdot \vec{\tau}_j + \frac{1}{4} n_i n_j \right]^{(\gamma)}, \tag{2}$$

where $\vec{\tau}_i^{\gamma} = \{\tau_{xi}^{\gamma}, \tau_{yi}^{\gamma}, \tau_{zi}^{\gamma}\}$ are pseudospin operators, acting in the subspace defined by the two orbitals which can be linked along a given γ direction.

For our purposes, it is convenient to characterize the correlations of each orbital flavor in terms of the no hole states $\hat{x}$, $\hat{y}$, and $\hat{z}$, standing for the local-orbital configurations having no hole in the corresponding orbital d_x, d_y, and d_z. For instance, if the bond is along the z axis, the virtual hopping connects $\hat{x}$ and $\hat{y}$ only, and the orbital interaction may be expressed via the Schwinger representation: $\tau_{+i}^c = p_{iy}^{\dagger} p_{ix}$, $\tau_{-i}^c = p_{ix}^{\dagger} p_{iy}$, $\tau_{zi}^c = \frac{1}{2}(n_{iy} - n_{ix})$, and $n_i^c = 2n_{iz} + n_{iy} + n_{ix}$, where $n_{i\gamma} = p_{i\gamma}^{\dagger} p_{i\gamma}$ and $p_{i\gamma}^{\dagger}$ and $p_{i\gamma}$ are creation and annihilation operators for $\hat{\gamma}$ configuration at site i. Similar relations with exchange of bond index hold for the other axis directions. Note that, to avoid any confusion with the pseudospin components, we renamed the orbital flavor $z=c$. Moreover, $J = 4t^2/U$, t being the hopping amplitude assumed equal for all the orbitals in the t_{2g} manifold, due to the symmetry relations of the connections via oxygen π ligands.[35,36]

It is worth to notice that, in absence of crystal field terms lifting orbital degeneracy, orbital exchange described by Hamiltonian in Eq. (2) is intrinsically frustrated: due to orbital singlets composition, antiferro-orbital correlations along x preclude exchange along y and vice versa. The result is a superposition of valence bond states which are uncorrelated along orthogonal directions.

Concerning the crystalline field contributions, H_{tet} is the tetragonal term linked to the compressive or tensile character of the c-axis octahedral distortions. In the no hole state representation, H_{tet} is written as follows:

$$H_{tet} = \Delta_{tet} \sum_i \left[n_{iz} - \frac{1}{2}(n_{iy} + n_{ix}) \right]. \tag{3}$$

Equation (3) implies that negative Δ_{tet} values lower the energy of $\hat{z}$ configurations, thus simulating a compressive distortion. This case is relevant for describing the short-c-axis insulating phase of $Ca_3Ru_2O_7$

The H_{ort} term describes in-plane orthorhombic deformations as due to a difference between the a and b crystallographic axis. From a general point of view, the orthorhombic deformations are introduced by means of the coupling between the orbital degree of freedom and the strain fields $\varepsilon_1 = \varepsilon_{xx} - \varepsilon_{yy}$ corresponding to a rotation axis such as [100] and $\varepsilon_2 = \varepsilon_{xy}$ corresponding to a rotation axis [110] in the tetragonal basis $[xyz]$. These distortions tend to lift the orbital degeneracy and thus can be viewed as effective orbital polarizing fields. From symmetry considerations,[28,37] one can show that a general form for the orthorhombic term can be expressed as follows:

$$H_{ort} = \sum_i (\Delta_{1,o} \tau_{zi}^c + \Delta_{2,o} \tau_{xi}^c). \tag{4}$$

where $\Delta_{1,o}$ and $\Delta_{2,o}$ correspond with the strain fields ε_1 and ε_2. Having in mind the orthorhombic distortions for the $Ca_3Ru_2O_7$ compound, where the RuO_6 octahedra are severely tilted in the ac plane thus rotated with respect to the b axis, one can assume that the $\Delta_{2,o}$ term is the relevant contribution to be included. Therefore, in our analysis the last term in Eq. (1) is just the following:

$$H_{ort} = \Delta_o \sum_i \tau_{xi}^c. \tag{5}$$

Still, negative values of Δ_o in H_{ort}, tend to stabilize a quantum state given by a superposition $\sim \hat{x} + \hat{y}$. This corresponds to select a preferential axial direction for orbital connectivity in the (a,b,c) frame that is obtained by performing a $(\pi/4, \pi/4, 0)$ rotation of (x,y,z) in real space. In the following we will refer to this as the "orthorhombic" frame and to the corresponding orbitals as d_a, d_b, and d_c.

Being interested in the response to an orbital only coupled field, we also include in the Hamiltonian of Eq. (1) the coupling between the external field and the local angular moment,[38] i.e.,

$$H_{\alpha} = 2B \sum_i \tau_{yi}^{\alpha}, \tag{6}$$

where B is the magnetic field coupled to the orbital degrees of freedom only in unit of Bohr magneton and $\alpha = a,b$ defines the direction, along which B is applied.

III. GROUND-STATE ORBITAL PATTERNS FOR A 2×2 PLAQUETTE

In this section we present the GS diagrams, obtained by means of an exact diagonalization study of the Hamiltonian above introduced on a 2×2 plaquette. As a strategy, we follow the evolution of the GS induced by the c axis compressive distortions, orthorhombic deformations and the ex-

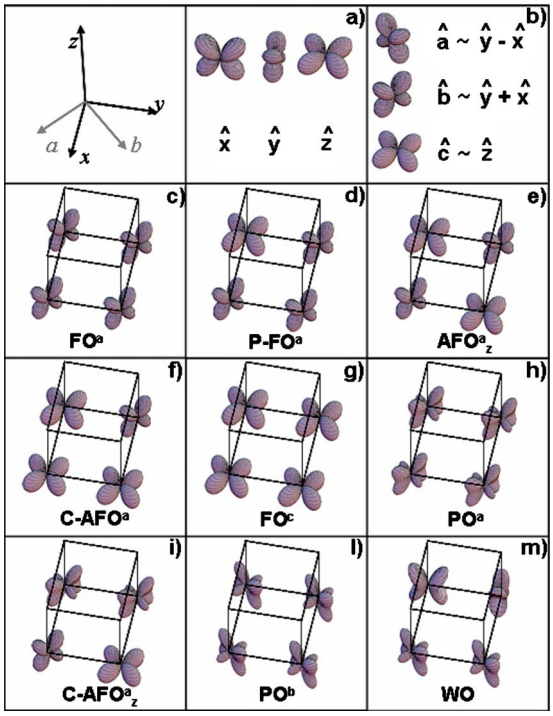

FIG. 1. (Color online) Schematic representation of the possible orbital patterns on a 2×2 plaquette, generated by the interplay between orbital exchange, tetragonal and orthorhombic distortions, applied orbital field. First panel shows the axis notation, panel (a) and panel (b) the graphical representation of $\hat{x},\hat{y},\hat{z}$ and $\hat{a},\hat{b},\hat{c}$ configurations, respectively. Panels (c)–(m) report the planar orbital pattern in terms of the local distribution of no-hole configurations; $\mathrm{FO}^{\alpha}/\mathrm{AFO}^{\alpha}$ stand for orbital patterns having homolog configurations on neighbors sites, for $\alpha=a,b,c$ flavor. P-FO stands for configurations with partial FO character, C-AFO for canted AFO. PO^{α} indicates paraorbital states where all pseudospins are τ_y^{α} oriented; WO stands for configurations characterized by a softening of AFO^{a} correlations, due to nonvanishing $\langle\tau_y^b\rangle$.

ternal orbital only field. The orthorhombic field is assumed in a way that the a direction is the easy-axis for the angular moments.

It turns out to be easier to characterize the different ground-state behaviors by evaluating the density and orbital correlators in the orthorhombic frame. We therefore introduce no hole configurations $\hat{a}$, $\hat{b}$, and $\hat{c}$, where the empty state is localized at d_a, d_b, and d_c, respectively. In Fig. 1(b), graphical representation of $\hat{a}$, $\hat{b}$, and $\hat{c}$, together with original $\hat{x}$, $\hat{y}$, and $\hat{z}$ [Fig. 1(a)] is reported. In terms of this new notation, it is easy to define the action of the pseudospin operators in the orthorhombic basis for the a,b,c flavors. For example, along the c axis, the pseudospin in the orthorhombic frame acts on $\hat{b}$ and $\hat{a}$ and it can be expressed via $\tau_{+i}^c=p_{ib}^{\dagger}p_{ia}$, $\tau_{-i}^c=p_{ia}^{\dagger}p_{ib}$, and $\tau_{zi}^c=\frac{1}{2}(n_{ib}-n_{ia})$.

Finally, in order to simplify the reading of the phase diagrams, we introduce the following notation: FO, AFO, WO stand for ferro-orbital (no-hole state on neighbors homolog orbitals), antiferro-orbital (no-hole state on neighbors off-diagonal orbitals), and weak antiferro-orbital correlations, respectively. Besides, P-FO stands for configurations with partial FO character, C-AFO for canted AFO while PO indicates the paraorbital high-field configuration. Furthermore, the superscripts (a,b,c) stand for the direction of the main contributions for the orbital correlators in terms of the pseudospins operators. The underscript (x,y,z) refers to the main character of the orbital correlations in the pseudospin space, i.e., it provides indication of the anisotropy of the orbital pattern. A schematic view of the representative orbital pattern configurations that contribute to the ground state on the 2×2 plaquette is reported in Figs. 1(c)–1(m), where the main component of the ground state is represented by means of the local-density distribution of no-hole configurations, in a way that a specific orbital on a given site stands for the local configuration having no holes in that orbital.

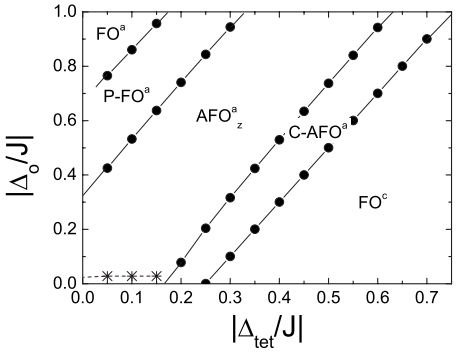

FIG. 2. Diagram summarizing the behavior of the GS configurations of a 2×2 cluster as a function of Δ_o/J and Δ_{tet}/J. Stars stand for smooth crossovers in the relevant correlators, solid dots for abrupt jumps. Phases are labeled in accordance to Fig. 1.

We notice that, except for the FO/AFO regions that are expected without explicit calculations, all the remaining phases are untrivial since they show an intermediate character, where the correlations have competing behaviors. For completeness, here we specify the way those regions are classified: (i) PO stands for the paraorbital uncorrelated high-field-configuration, driven by the field H_{α}, where the pseudospins are τ^{α} oriented and the correlators $\langle\tau_i^{\alpha}\tau_j^{\alpha}\rangle$, evaluated in the orthorhombic frame, have the maximum saturated value of 0.25 [see, for example, Figs. 10(a) and 11(b)]; (ii) generic C-AFO stand for regions where nearest-neighbor antiferro-orbital correlations characterizing AFO are strongly suppressed and coexist with FO components, as shown for example in Fig. 10. (iii) WO has the feature of an isotropic weak antiferro-orbital phase, obtained when the field is applied along the hard axis b, resulting from a reduction in the nearest-neighbors $\langle\tau_{yi}^a\tau_{yj}^a\rangle$ antiferro-type correlations due to a nonvanishing onsite momentum τ_y^b. In this region, FO and AFO correlations are the same order of magnitude, as shown in Fig. 11, meaning that no preferred behavior can be identified.

A. Effect of structural distortions

As a first step we discuss the case at zero applied field. In Fig. 2, the ground-state diagram is shown, obtained by varying the crystal-field microscopic parameters Δ_{tet} and Δ_o in unit of J. It turns out to be convenient to span the different

regions of Fig. 2 by fixing an ideal horizontal line corresponding to, e.g., $|\Delta_o/J|=0.8$ while varying the tetragonal parameter.

Tetragonal crystal field acts as an effective orbital bias that tunes the density of $\hat{c}$ configurations from 0 to 1, corresponding to weak and strong regime of compressed octahedra, respectively. Looking at the relevant correlation functions, we see that the two ending regions are both characterized by a complete quenching of the orbital correlations. In the weak tetragonal regime, the orthorhombic field is strong enough to give rise to a complete FO^a (see Fig. 1, panel c), where stabilizing $\hat{b}$ configurations generates full FO correlations for the τ_z^a components. In the extreme flattened RuO_6 regime, instead, we get a FO^c region (see Fig. 1, panel c), where the ferro-orbital correlations are saturated along the z direction for the flavor c.

These two regions are linked by intermediate regions characterized by a partial filling of the t_{2g} subspace. We highlight that, due to the constraint of the planar geometry, and that of the orthorhombic field favoring $\hat{b}$ configurations, the orbital interaction along b, involving $\hat{a}$ and $\hat{c}$, is inactive thus yielding an anisotropic effect between a and b directions.

Particularly, in the regime of intermediate tetragonal field, $0.2<|\Delta_{tet}/J|<0.4$, we find an AFO_z^a region, represented in Fig. 1(e), characterized by the alternation of $\hat{c}$ and $\hat{b}$, that gives rise to predominant AFO correlations along z direction, for flavor a. This region is interesting when compared with the magnetic/orbital pattern in $Ca_3Ru_2O_7$; indeed, the occurrence of an AFO pattern can explain, in a spin/orbital picture, the existence of ferromagnetic in-plane correlations, and it can be also related to the poorly metallic behavior of the GS, as due to an OO pattern. We finally remark that, in the AFO_z^a, the order of magnitude of the x,y,z correlators for the a flavor is comparable, though the amplitude for the z channel is larger than the others.

B. Interplay between structural distortions and orbital polarizing field

1. Easy axis

Let us now discuss the interplay between the structural distortions and the effects of a polarizing field. In doing that, we consider just one representative value for the orthorhombic strain $|\Delta_o/J|=0.4$. This is the most interesting regime where the structure of the ground state is more sensitive to external small perturbations. This would permit to explore the modifications induced on the corresponding line of Fig. 2, and particularly of the region at the boundary between AFO^a and FO^c, occurring for intermediate/strong tetragonal crystal-field amplitude.

Due to the anisotropy introduced by the orthorhombic field, we distinguish between the response along the a and b directions. The corresponding ground-state diagrams are displayed in Figs. 3 and 4. The investigation of these diagrams will be confined to the low fields regime since, approaching high fields, the orbital momentum becomes fully polarized, as in the PO^a region of Fig. 1(h), resulting from stabilizing $\sim(\hat{b}+i\hat{c})$, or the PO^b region of Fig. 1(i), corresponding to

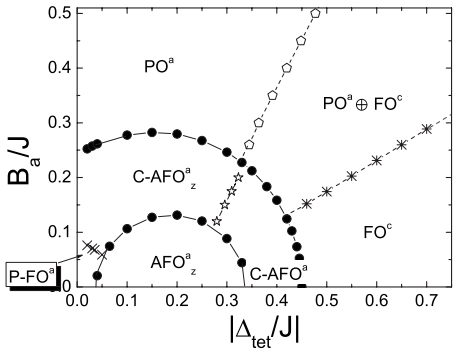

FIG. 3. Ground-state diagram of a 2×2 cluster obtained for an orbital-only applied field along the easy axis a as a function of $|\Delta_{tet}/J|$, for a fixed value $|\Delta_o/J|=0.4$. Dots correspond to abrupt jumps in the evolution of the relevant off-site orbital correlators; stars and diamonds to smooth crossover in the correlation functions. Different regions are labeled according to Fig. 1.

$\sim(\hat{c}-i\hat{a})$ local configurations. We do believe that, in this limit, the assumption of neglecting the spin magnetization becomes weak and thus an analysis of the complete spin-orbital effective model is required.

Figure 3 shows the occurrence of crossovers in the orbital correlators among different GS configurations generated for $B\|a$. We do notice a peculiar evolution of the boundary for the AFO_z^a state. Indeed, aligning the moment along y for the a flavor, regions AFO^a and FO^c move toward a new regime where AFO^a along y is partially reduced evolving into a cantedlike state $C\text{-}AFO_z^a$ [see Fig. 1, panel (i)], with a nonzero total angular momentum, directed along y, coexisting with partial AFO^a correlations along z.

2. Hard axis

The response for $B\|b$ is instead more stiff (see Fig. 4). In Fig. 5, we give a schematic representation of the action of pseudospin operators on different orbital subspaces: the ground state at zero field is a combination of $\hat{b}$ and $\hat{c}$ states and the application of the field along b induces $\hat{a}$-type configurations that are unfavored with respect to the orthorhom-

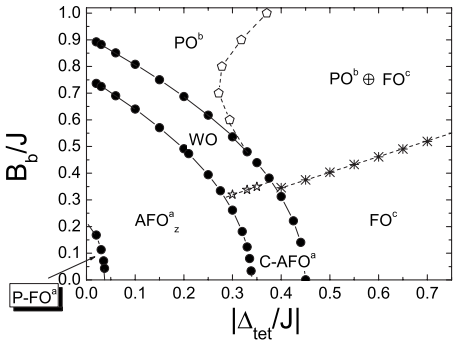

FIG. 4. Ground-state diagram of a 2×2 cluster obtained for an orbital-only applied field along the hard axis b as a function of $|\Delta_{tet}/J|$, for a fixed value $|\Delta_o/J|=0.4$. Dots correspond to abrupt jumps in the evolution of the relevant off-site correlators; stars and diamonds to smooth crossover. The regions are labeled according to Fig. 1.

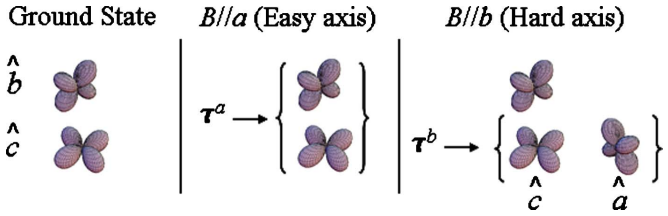

FIG. 5. (Color online) Schematic representation of orbital configurations activated by an applied orbital field. Left panel shows $\hat{b}$ and $\hat{c}$ orbital configurations set by the interplay between crystal field amplitudes. Middle panel shows the orbital subspace where τ^a is active; right panel shows the orbital subspace where τ^b is active. The orbital field, applied along hard axis b, restores orbital fluctuations among the whole orbital subspace by reintroducing $\hat{a}$ configurations.

bic deformations. This implies that a much higher value of the field is required to activate the orbital exchange along b. Along this symmetry direction, the orbital polarizing field tends to restore a description where all the three t_{2g} flavors are active. Due to the new configurations $\hat{a}$, and to the competing mechanisms involved, the resulting effect is a weakly ordered WO configuration. Such state is marked by a coexistence between AFO correlations along a and FO along b [see Fig. 1, panel (m)].

Now, comparing the response of the system for the different field directions in the interval of crystal field given by about $0.1 < |\Delta_{tet}/J| < 0.5$, one can observe that, if the field is along the a axis, the closest configurations that can be activated, starting from AFO^a and FO^c, still have an OO pattern as given by $\mathrm{C/AFO}^a$. On the contrary, for $B \| b$, due to the activation of the b flavor, we get a changeover from an OO pattern to an WO configuration.

This analysis shows that when AFO and FO configurations are close in energy, the application of the external field may act as a tunable parameter within the orbital configurations, thus suggesting that the complex field response in the bilayered ruthenate may be consequence of the subtle interplay between different microscopic mechanisms that involve the orbital couplings and the fields associated with the octahedral deformations in presence of large Coulomb coupling. One of the main findings is the occurrence of an orbital ordered pattern at the boundary between FO and AFO states, stabilized when the field is along the easy axis, as due to the effective freezing of one orbital flavor. When the field is applied along the hard axis, quantum fluctuations associated with the three-orbital degrees of freedom are restored and tend to destroy the orbital ordering.

IV. CLUSTER EMBEDDED CALCULATION

In this section we extend the cluster calculation considering the case of a four-site plaquette embedded in a periodic environment as schematically represented in Fig. 6. Here, the intraplaquette Hamiltonian is solved via exact diagonalization and the interplaquettes interaction is treated within a self-consistent mean-field approximation.

Indeed, the MF scheme of analysis corresponds to decouple the interplaquette terms of the Hamiltonian as it follows:

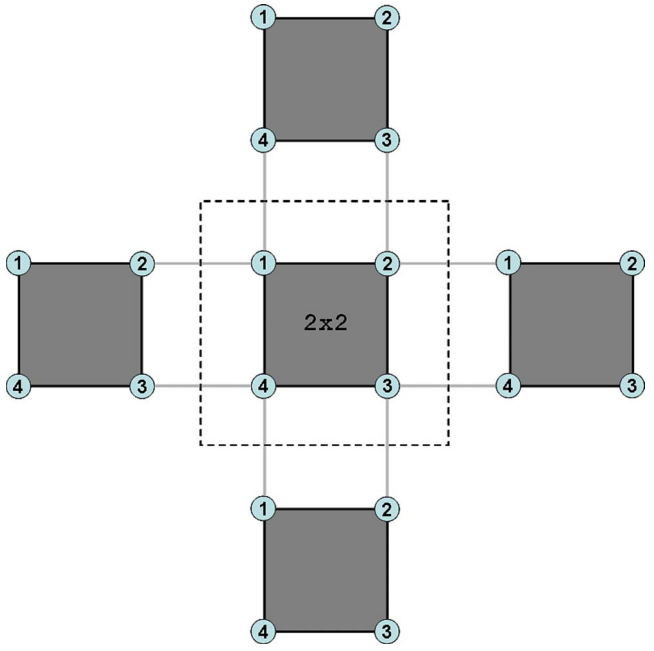

FIG. 6. (Color online) Schematic representation of a 2×2 cluster embedded in a periodic environment. Filled square denotes 2×2 plaquette described by Eq. (1), whose interaction with the field produced by four surrounding empty squares is expressed by Eq. (7). Dashed square defines the basic unity of the periodic structure.

$$H_{exc} = J \sum_{\gamma=x,y} \sum_{\mu=x,y,z} \sum_{\langle ij \rangle \| \gamma} \left[\tau_i^\mu \langle \tau_j^\mu \rangle + \frac{1}{4} n_i \langle n_j \rangle \right]^{(\gamma)} - J \sum_{\gamma=x,y} \sum_{\mu=x,y,z} \sum_{\langle ij \rangle \| \gamma} \left[\langle \tau_i^\mu \rangle \langle \tau_j^\mu \rangle + \frac{1}{4} \langle n_i \rangle \langle n_j \rangle \right]^{(\gamma)} \quad (7)$$

where γ stands for the axial direction and μ for the pseudospin component. Hence, Eq. (7) represents the exchange interaction between the plaquette and the nearest-neighbors sites in the (x,y) plane, treated on a mean field level. Here, the average $\langle \cdots \rangle$ of the local pseudospin operators is determined after solving the full quantum problem within the plaquette. The decoupling of the orbital exchange on nearest-neighbor plaquettes tends to prefer broken symmetry states with AFO correlations. This tendency is in competition with the local distortive fields due to the octahedral distortions and is strongly related to the intraplaquette quantum effects. Hence, the solution is determined in a self-consistent fashion, according to the following scheme: we assign initial conditions for $\langle \vec{\tau}_i^\gamma \rangle$ and $\langle n_i^\gamma \rangle$, and use them to evaluate improved expectation values; the procedure runs until convergence is achieved, with the requested accuracy. This scheme is applied for all the different initial conditions associated with possible orbital states emerging from ED on the four-site plaquette. In particular, we consider all the starting configurations where local pseudospins are oriented along a given direction and FO, A-FO, C-AFO, and WO correlated, and we finally choose the lowest energy orbital configuration among the ones self-consistently obtained. Mean field drives the solution toward broken symmetry states having a specific orbital pattern that can be characterized by local order pa-

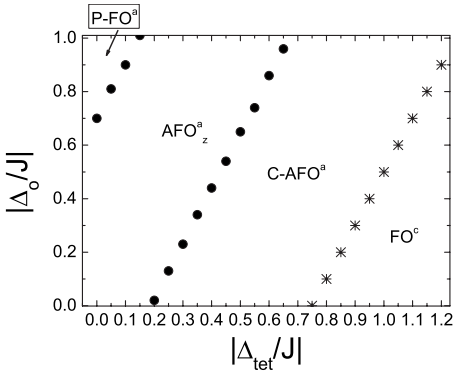

FIG. 7. Diagram summarizing the behavior of the GS configurations as a function of Δ_o/J and Δ_{tet}/J for a cluster embedded in a periodic environment.

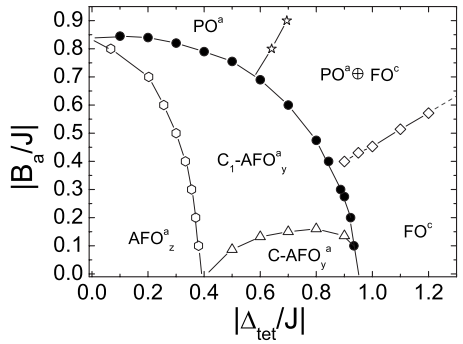

FIG. 8. Diagram summarizing the behavior of the GS configurations as a function of Δ_{tet}/J and B_a/J, for a cluster embedded in a periodic environment at $|\Delta_o/J|=0.4$.

rameters $\langle \vec{\tau}_i^{\gamma} \rangle$, and by explicitly evaluating orbital correlations developing along different axial direction of the orthorhombic frame. We point out that this feature is not intrinsic in the MF approach but is strongly related to the anisotropic microscopic environment due to crystal field terms. The latter break rotational invariance in the pseudospin space, allowing solutions with a specific orbital patterns to be stabilized.

We finally remark that, by exploring broken symmetry states with defined OO patterns, we can get informations about the thermodynamic stability of the corresponding OO phases.

A. Effect of structural distortions

We first consider the MF evolution starting from orbital configurations of a 2×2 plaquette at zero applied field. We look for most stable solutions, chosen among those having FO-AFO and C/AFO character. In Fig. 7, we show the phase diagram as a function of the tetragonal and orthorhombic crystal field amplitudes. When comparing this diagram to the cluster calculation (Fig. 2), the following features emerge: (i) the value of $|\Delta_{tet}/J|$ separating AFO_z^a and C-AFO^a regions is not modified by the MF and scales with $|\Delta_o/J|$ according to the same linear law; (ii) in the moderately/highly flattened region, the most stable solution has a C-AFO^a character. Looking at orbital correlations in the orthorhombic frame, this corresponds to AFO correlations in x,y components of flavor a coexisting with FO correlations for τ_z^a. Approaching the extremely flattened side, the AFO correlations for $\tau_{x,y}^a$ are gradually replaced by the FO character of τ_z^a τ_z^b, which is saturated reaching FO^c. Moreover τ_x^c is decreasing and FO correlated. (iii) In the regime of strong orthorhombic field, we observe that the full FO^a is no more stable and leaves the place to a region having a uniform P-FO^a character (the evolution of the expectation values as a function of the orthorhombic field suggests that FO^a is stabilized for higher values of $|\Delta_o| \gtrsim 2$). This configuration is somehow symmetric with respect to C-AFO^a but has an inverted balance between $|\hat{z}\rangle$ and $(\hat{x},\hat{y})$ sector. (iv) In the AFO_z^a the self-consistence leads to a state with pure z components of the a and b flavor (correlations along x and y renormalize down to zero while they were not vanishing for the uncoupled cluster case).

B. Effect of orbital-only applied field

1. Easy axis

The effect of a polarizing field along easy axis a is to induce a nonvanishing y component of local orbital momentum $\langle \tau_y^a \rangle$. This anisotropic effect is thus relevant for the evolution of the C-AFO^a, where AFO^a correlations exist both for the x and y components. Therefore, we expect that the polarizing field naturally will select the latter. Moreover it's interesting to see how the induced FO correlations compete with the general tendency toward AFO. In Fig. 8, we report the evolution of the line $|\Delta_o/J|=0.4$ of Fig. 7, as a function of the applied field. As one can see, one of the main differences, with respect to the four-site plaquette calculation (see Fig. 3), is that now most of the transitions occur as a smooth crossover in the relevant correlators, represented by empty dots and stars (see Fig. 10).

High-field regions are uninteresting (PO phases are stabilized), so we skip them in the discussion. In the low $|\Delta_{tet}/J|$ region, we see that the AFO_z^a region remains quite stable and the effect of the polarizing field is to progressively orient the local orbital momentum from z to y. The main modifications occur in the moderately flattened region where the C-AFO region–that now has broken symmetry, being active only for y component leaves place to $\mathrm{C_1\text{-}AFO}_y^a$. This region has the features of a strengthened OO, where $\hat{c}$ and $\hat{a}$ configurations alternate along the bonds [see Fig. 9(d)]. Looking at orbital correlators in Figs. 10(a) and 10(b), we deduce that in this region the competition between crystal field amplitude and applied field has the effect to suppress nearest neighbors exchange. The OO that is stabilized has a strong FO character along opposite diagonals for τ_y^a and τ_z^a, respectively, as shown by next nearest neighbors correlations, which are almost saturated to a value of ~ 0.25.

To clarify the mechanism leading to the suppression of AFO correlations, we point out that the characteristic energy scale is on the order of J. The analogy with an Heisenberg antiferromagnet, disordered by an applied magnetic field, suggests that orbital correlations are tuned by the interplay between applied field and orbital exchange, in a way that is

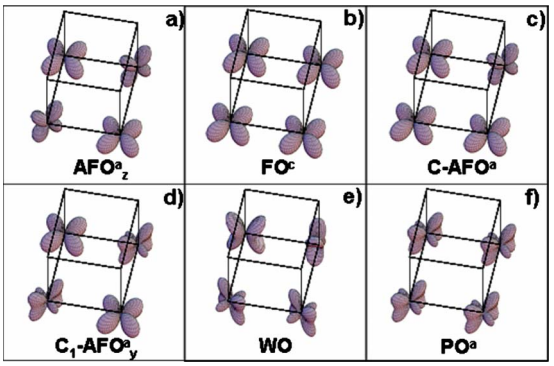

FIG. 9. (Color online) Schematic representation of possible orbital patterns for a 2×2 cluster embedded in a periodic environment as due to the interplay between orbital exchange, tetragonal and orthorhombic distortions, and applied orbital field. Panels (a)–(f) report the planar orbital pattern in terms of the local distribution of 'no-hole' configurations; FO$^\alpha$/AFO$^\alpha$ stand for orbital patterns having homolog configurations on neighbors sites, for $\alpha=a,b,c$ flavor. C-AFO for canted AFO. PO$^\alpha$ indicates paraorbital states where all pseudospins are τ_y^α oriented; WO stands for configurations characterized by a softening of AFO^a correlations, due to nonvanishing $\langle\tau_y^b\rangle$

not dependent on the crystal field amplitude, once the orthorhombic deformations have selected the "easy flavor" a.

2. Hard axis

When the field is applied along the hard axis b, a stronger intensity than that for the a case is required to stabilize the full PO region. The evolution toward PO is the result of the smooth suppression of AFO correlations, as demonstrated by the suppression of $\langle\tau_{y_i}^a\tau_{y_j}^a\rangle$ between nearest neighbors [see Fig. 11(a)]. In the regime $0.4<|\Delta_{tet}/J|<0.6$, at the boundary between AFO$_z^a$ and C-AFO$_y^a$, this determines a WO behavior, represented in Fig. 9(e). This region is the result of disordering C-AFO^a by introducing a nonvanishing onsite momentum $\langle\tau_y^b\rangle$ along the hard axis direction. As we already pointed out in previous section, this corresponds to restore orbital fluctuations along b by introducing $\hat{a}$ configurations, as illustrated in Fig. 5. Reactivating fluctuations in the whole orbital subspace, brings the system back to a situation where frustration of the orbital exchange is enhanced.

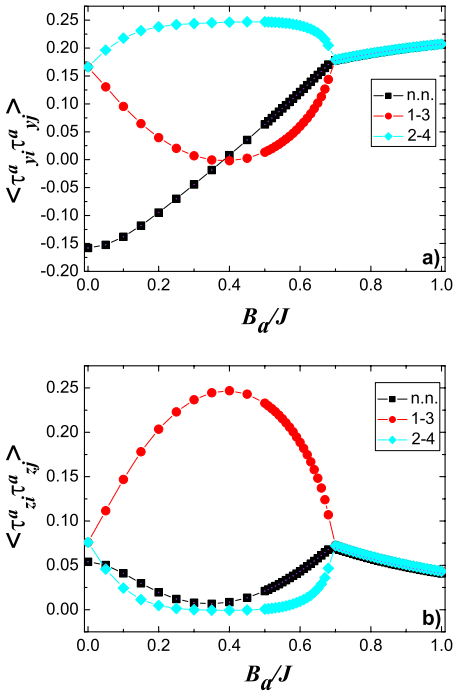

FIG. 10. (Color online) Expectation value of orbital correlators in the orthorhombic frame as a function of applied field, evaluated for $|\Delta_{tet}/J|=0.6$ and $|\Delta_o/J|=0.4$. Panels (a) and (b) show dominant contributions arising when the field is applied along easy axis.

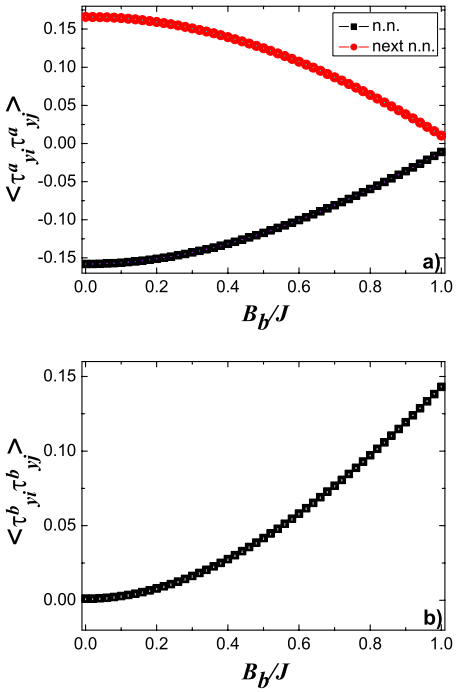

FIG. 11. (Color online) Expectation value of orbital correlators in the orthorhombic frame as a function of applied field, evaluated for $|\Delta_{tet}/J|=0.6$ and $|\Delta_o/J|=0.4$. Panels (a) and (b) show dominant contributions arising when the field is applied along hard axis.

We notice that, contrary to the easy axis case, for the hard axis orbital exchange between nearest neighbors is not hindered. Moreover, we remark that the energy scale stabilizing WO is now strongly related to the crystal-field amplitudes. We explored the evolution of region boundaries in Fig. 12, and found that the onset of WO region grows linearly with Δ_o. These aspects underline that the softening of AFO correlations is here caused by the reduction in onsite orbital momentum due to the new activated flavor, instead of by the field-induced FO correlations.

V. CONCLUSIONS

We have here presented a study of field tunability of orbital correlations for layered ruthenates in an insulating ferromagnetic configuration. We have analyzed the evolution of the possible orbital patterns under the effect of the external

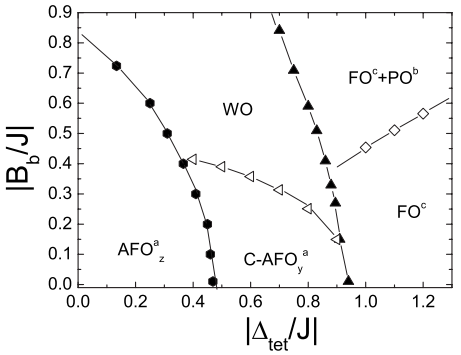

FIG. 12. Diagram summarizing the behavior of the GS configurations as a function of Δ_{tet}/J and B_b/J, for a cluster embedded in a periodic environment at $|\Delta_o/J|=0.4$.

magnetic field coupled to the local angular momentum only. Numerical calculations on a 2×2 cluster and of a cluster embedded in a periodic environment reveal that the competing effects driven by orbital exchange and crystal field put the system on the verge of a FO/AFO behavior, a circumstance that makes the character of OO in absence of an applied field quite elusive. This outcome may be supported by recent resonant x-ray scattering measurements on $Ca_3Ru_2O_7$,[39] where no appreciable signal of staggered FO or AFO is found within experimental resolution. We argue that this feature is at the origin of the soft behavior and the easy field tunability of the OO phases. Particularly, AFO exchange leaves the place to strong next-nearest-neighbors FO correlations when an external orbital field is applied along the easy axis while we get a tendency to an isotropic weak antiferro-orbital correlated state for the hard axis. An interpretation of these results can be summarized as follows: the orthorhombic deformations tend to remove the orbital degeneracy and lead to an ordered state where only two local t_{2g} configurations are active. The effect of the polarizing field is to keep the orbital correlations in the two-orbital sector when the field is along easy-axis; otherwise, along the hard-axis the field forces the system to allow for all possible local orbital fluctuations. The latter situation is responsible for demolishing the OO ground state set by the competition between Coulomb and crystal-field interactions. Speaking on a general ground, in many multiorbital Mott insulators the metal-insulator transition occurs as a symmetry breaking phase transition leading to magnetic, orbital and charge orderings. We speculate that a possible connection may exist between the demolition of long range OO by an applied field and a likely metallic behavior and that this connection may be of interest when referred to unconventional magneto-conducting properties of $Ca_3Ru_2O_7$.

We finally point out some important remarks about a quantitative connection of our calculation to the physical parameters regime expected in the layered ruthenates, and specifically of $Ca_3Ru_2O_7$. According to our results, the evolution of region boundaries between AFO, C-AFO, or WO behaviors is mainly concentrated within the windows $0.2<\Delta_{tet}/J<0.8$ and $0.1<\Delta_o/J<0.4$. Checking the range of the microscopic parameters that bias the proposed orbital patterns is not easy since the amplitude of J, Δ_{tet}, and Δ_o is difficult to be directly measured and require a model derivation. An explicit *ab initio* evaluation for $Ca_3Ru_2O_7$ is not yet available. For the closest members of Ruddlesden-Popper series according to their physical and structural properties, Ca_2RuO_4 and $Sr_3Ru_2O_7$, respectively, one ends up with the following *ab-initio* estimates $J\sim50$ meV, $\Delta_{tet}\sim20$ meV and $\Delta_o\sim5$ meV.[40,41] These values set the ratios $\Delta_{tet}/J\sim0.4$ and $\Delta_o/J\sim0.1$, whose orders of magnitude are compatible with our choices of analysis for the regions of phase diagrams where major changes occur.

[1] S. Maekawa, T. Tohyama, S. E. Barnes, S. Ishihara, W. Koshibae, and G. Khaliullin, *Physics of Transition Metal Oxides* (Springer-Verlag, Berlin, 2004).
[2] Y. Tokura and N. Nagaosa, Science **288**, 462 (2000).
[3] M. Imada, A. Fujimori, and Y. Tokura, Rev. Mod. Phys. **70**, 1039 (1998).
[4] E. Dagotto, T. Hotta, and A. Moreo, Phys. Rep. **344**, 1 (2001); E. Dagotto, New J. Phys. **7**, 67 (2005); *Physics of Manganites*, edited by T. A. Kaplan and S. D. Mahanti (Kluwer Academic, Dordrecht, 1999).
[5] E. Dagotto, *Nanoscale Phase Separation and Colossal Magnetoresistance*, Springer Series in Solid State Sciences Vol. 136 (Springer-Verlag, Heidelberg, 2003).
[6] L. F. Feiner, A. M. Oles, and J. Zaanen, Phys. Rev. Lett. **78**, 2799 (1997).
[7] G. Khaliullin and V. Oudovenko, Phys. Rev. B **56**, R14243 (1997); G. Khaliullin and R. Kilian, J. Phys.: Condens. Matter **11**, 9757 (1999).
[8] G. Khaliullin, P. Horsch, and A. M. Oles, Phys. Rev. Lett. **86**, 3879 (2001); P. Horsch, G. Khaliullin, and A. M. Oles, *ibid.* **91**, 257203 (2003).
[9] G. Khaliullin and S. Maekawa, Phys. Rev. Lett. **85**, 3950 (2000).
[10] G. Cao, L. Balicas, Y. Xin, E. Dagotto, J. E. Crow, C. S. Nelson, and D. F. Agterberg, Phys. Rev. B **67**, 060406(R) (2003).
[11] G. Cao, L. Balicas, X. N. Lin, S. Chikara, E. Elhami, V. Duairaj, J. W. Brill, R. C. Rai, and J. E. Crow, Phys. Rev. B **69**, 014404 (2004).
[12] H. L. Liu, S. Yoon, S. L. Cooper, G. Cao, and J. E. Crow, Phys. Rev. B **60**, R6980 (1999).
[13] X. N. Lin, Z. X. Zhou, V. Durairaj, P. Schlottmann, and G. Cao, Phys. Rev. Lett. **95**, 017203 (2005).
[14] J. F. Karpus, R. Gupta, H. Barath, S. L. Cooper, and G. Cao, Phys. Rev. Lett. **93**, 167205 (2004).
[15] J. F. Karpus, C. S. Snow, R. Gupta, H. Barath, S. L. Cooper, and G. Cao, Phys. Rev. B **73**, 134407 (2006).
[16] G. Cao, K. Abbound, S. McCall, J. E. Crow, and R. P. Guertin, Phys. Rev. B **62**, 998 (2000).
[17] E. Ohmichi, Y. Yoshida, S. I. Ikeda, N. Shirakawa, and T. Osada, Phys. Rev. B **70**, 104414 (2004).
[18] C. S. Nelson, H. Mo, B. Bohnenbuck, J. Strempfer, N.

Kikugawa, S. I. Ikeda, and Y. Yoshida, Phys. Rev. B **75**, 212403 (2007).
[19] S. McCall, G. Cao, and J. E. Crow, Phys. Rev. B **67**, 094427 (2003).
[20] Y. Yoshida, S. I. Ikeda, H. Matsuhata, N. Shirakawa, C. H. Lee, and S. Katano, Phys. Rev. B **72**, 054412 (2005).
[21] Here we refer to the notation adopted by Cao and coworkers in Ref. 16. On the contrary, neutron diffraction data (Ref. 20) and x-ray scattering studies (Ref. 18) report *b* as low-temperature easy axis.
[22] G. Cao, L. Balicas, Y. Xin, J. E. Crow, and C. S. Nelson, Phys. Rev. B **67**, 184405 (2003).
[23] Z. Qu, J. Peng, T. Liu, D. Fobes, L. Spinu, and Z. Mao, Phys. Rev. B **80**, 115130 (2009).
[24] J. Spalek and W. Wojcik, *Spectroscopy of Mott Insulators and Correlated Metals* (Springer, Berlin, 1995).
[25] D. Duffy and A. Moreo, Phys. Rev. B **55**, R676 (1997).
[26] V. Dobrosavljević and G. Kotliar, Philos. Trans. R. Soc. London, Ser. A **356**, 57 (1998).
[27] J. S. Lee, S. J. Moon, B. J. Yang, Yu. Jaejun, U. Schade, Y. Yoshida, S.-I. Ikeda, and T. W. Noh, Phys. Rev. Lett. **98**, 097403 (2007).
[28] V. I. Anisimov, I. A. Nekrasov, D. E. Kondakov, T. M. Rice, and M. Sigrist, Eur. Phys. J. B **25**, 191 (2002).
[29] M. Neupane, P. Richard, Z.-H. Pan, Y.-M. Xu, R. Jin, D. Mandrus, X. Dai, Z. Fang, Z. Wang, and H. Ding, Phys. Rev. Lett. **103**, 097001 (2009).
[30] L. de' Medici, S. R. Hassan, M. Capone, and X. Dai, Phys. Rev. Lett. **102**, 126401 (2009).
[31] P. Werner, E. Gull, and A. J. Millis, Phys. Rev. B **79**, 115119 (2009).
[32] J. Kurmann, G. Müller, H. Thomas, M. W. Puga, and H. Beck, J. Appl. Phys. **52**, 1968 (1981).
[33] M. Kenzelmann, R. Coldea, D. A. Tennant, D. Visser, M. Hofmann, P. Smeibidl, and Z. Tylczynski, Phys. Rev. B **65**, 144432 (2002).
[34] D. V. Dmitriev and V. Ya. Krivnov, Phys. Rev. B **70**, 144414 (2004).
[35] M. Cuoco, F. Forte, and C. Noce, Phys. Rev. B **74**, 195124 (2006).
[36] M. Cuoco, F. Forte, and C. Noce, Phys. Rev. B **73**, 094428 (2006).
[37] M. Sigrist and M. Troyer, Eur. Phys. J. B **39**, 207 (2004).
[38] K. Yoshida, *Theory of Magnetism* (Springer, Heidelberg, 1996).
[39] B. Bohnenbuck, I. Zegkinoglou, J. Strempfer, C. Schüßler-Langeheine, C. S. Nelson, Ph. Leininger, H.-H. Wu, E. Schierle, J. C. Lang, G. Srajer, S. I. Ikeda, Y. Yoshida, K. Iwata, S. Katano, N. Kikugawa, and B. Keimer, Phys. Rev. B **77**, 224412 (2008).
[40] E. Gorelov, M. Karolak, T. Wehling, F. Lechermann, A. Lichtenstein, and E. Pavarini, Phys. Rev. Lett. **104**, 226401 (2010).
[41] E. Pavarini (private communication).